Modelling water wave overwash of a thin floating plate

D. M. Skene[1], L. G. Bennetts[1], M. H. Meylan[2], A. Toffoli[3]

[1]School of Mathematical Sciences, University of Adelaide, Adelaide 5005, Australia

[2]School of Mathematical and Physical Sciences, University of Newcastle, Callaghan 2308, Australia

[3]Centre for Ocean Engineering Science and Technology, Swinburne University of Technology, Melbourne 3122, Australia

September 10, 2015

Abstract

A theoretical model of water wave overwash of a thin floating plate is proposed. The nonlinear shallow water equations are used to model the overwash, and the linear potential-flow/thin-plate model to force it. Model predictions are compared to overwash depths measured during a series of laboratory wave basin experiments. The model is shown to be accurate for incident waves of low steepness or short length.

1 Introduction

Thin floating plates are conventionally used to model sea ice floes in theoretical models of ocean surface wave propagation through the ice-covered ocean (see the review of Squire, 2007). The models are now being integrated into large-scale, numerical, ice/ocean models to predict wave penetration distances into the ice-covered ocean (e.g. Doble & Bidlot, 2013) and concomitant wave-induced breakup of the ice cover (e.g. Dumont *et al.*, 2011).

A theoretical model of a water wave interacting with a solitary plate is the kernel of the wave-ice models. The incident wave and plate lengths are comparable, i.e. the wave and plate motions are strongly coupled. Potential-flow theory models water motions, and, typically, Kirchhoff-Love theory models the plate motions. The model incorporates the plate's elastic response via its Young's modulus. Thus, it extends classic models of wave-body interactions, for example, models of ship hydrodynamics.

Moreover, it is customarily assumed that wave amplitudes are sufficiently small to employ linear theory. Meylan & Squire (1994) developed the first solution method for the full-linear problem in two spatial dimensions. Bennetts & Williams (2010), amongst others, developed a solution method for the extended three-dimensional problem.

Laboratory experimental validation of the solitary plate model is a relatively recent development. Montiel *et al.* (2013*a*,*b*) used a series of wave tank experiments on polyvinyl chloride (PVC) plastic disks with regular incident waves of low steepness to validate the linear model. However, they installed vertical barriers around the edges of the disk to prevent the waves overwashing them, and hence maintain consistency with the theoretical model.

Overwash refers to water running over the top of the plate, forced by the surrounding wave motion. It occurs for moderate incident amplitudes, due to the small freeboard of the thin plate. It is a highly nonlinear phenomenon, and is not included in the handful of existing nonlinear theoretical models (e.g. Papathanasiou *et al.*, 2015).

Overwash is related to green water, i.e. water loads on ship decks and other offshore structures, forced by large storm waves. Mizoguchi (1989) first proposed a theoretical model of green water, based on the shallow-water dam-break model. Buchner & Cozijn (1997) and Greco (2001), amongst others, have since significantly developed and validated green water models. However, overwash distinguishes

itself from green water by (i) occuring for moderate incident wave amplitudes, and (ii) being semi-continuously forced, as opposed to the 'first event' nature of green water.

In an investigation closely related to the present one, Meylan *et al.* (2015) validated the linear model predictions of plate motions using experiments on solitary plates without edge barriers. They used square plates made of PVC and a denser and more rigid polypropylene (PP) plastic. They showed that the linear model is accurate for a range of incident wave lengths and steepnesses, even in cases where strong overwash occurred. Bennetts *et al.* (2015) analysed the wave fields transmitted by the plates during the experiments. They showed that as the incident wave steepness increases the transmitted wave becomes irregular and the proportion of wave energy transmitted decreases. They noted that the steeper incident waves concomitantly produced strong overwash.

Bennetts & Williams (2015) validated two theoretical models of wave transmission by multiple thin plates, using wave basin experiments on 40 to 80 wooden disks. They noted a correlation between strong overwash and a reduction in the proportion of wave energy transmitted by the disks, and hence a loss of model accuracy.

The works cited above used the experimental measurements to assess model accuracy at basin scale. A Froude scaling, with a specified geometric scaling factor, is typically used to interpret the measurements at field scale. In particular, density does not change from basin to field scales. The PP plastic used by Meylan *et al.* (2015) has a density that closely matches measured values for sea ice, and its freeboard is therefore representative of the freeboard of natural ice floes. PVC has a lower density than sea ice and, thus, its freeboard is greater than that of ice floes. The elastic modulus must be multiplied by the geometric scaling factor to obtain the equivalent field value. Plastic plates are generally more rigid than ice floes at field scale, although the more compliant PVC is representative of ice floes up to geometrical scaling factors of approximately 20.

Here, a theoretical model of overwash is proposed. Following green water models, the nonlinear shallow water equations model the overwash. The surrounding water and plate motions predicted by the linear model force the overwash, with no back coupling from the overwash to the surrounding water or plate motions. This model assumption is motivated by the findings of Meylan *et al.* (2015). A dataset from the same experimental campaign used by Meylan *et al.* (2015) is used to validate the overwash model. The dataset derives from tests using the same plates and range of incident wave lengths and steepnesses. However, overwash depths, rather than the motions of the plates, were measured.

2 Wave basin experiments

Experiments were conducted in the wave basin facility of the Coastal Ocean and Sediment Transport (COAST) Laboratory, Plymouth University, U.K. The basin is 10 m wide, 15.5 m long and filled with fresh water of density $\rho \approx 1000\,\mathrm{kg\,m^{-3}}$ and $H = 0.5\,\mathrm{m}$ depth. Figure 1 shows a schematic plan view of the basin. At the right-hand end of the basin a piston controlled wave maker is used to generate incident waves and absorb a proportion of the waves reflected back to it. A beach at the left-hand end of the basin absorbs the majority of the wave energy that reaches it. A reflection analysis was conducted at the centre of the basin prior to the full tests. It showed the combination of the beach and absorption by the wave maker resulted in reflected wave energy contributing less than 1% to the overall wave energy.

For each test, a solitary thin floating plastic plate was deployed in the basin. All plates used were square with side lengths $2L = 1\,\mathrm{m}$. They were loosely tethered at their corners to the basin floor. The tether had a natural period greater than 20 s, which is over an order of magnitude greater than the period of the incident waves used. It allowed the plates to surge back and forth at the period of the incident waves but restricted drift down the basin.

Both PP and PVC plastics were used. The PP had a manufacturer specified density $\rho_\mathrm{p} = 905\,\mathrm{kg\,m^{-3}}$ and elastic modulus $E = 1600\,\mathrm{MPa}$. The PVC had manufacturer specified density $\rho_\mathrm{p} = 500\,\mathrm{kg\,m^{-3}}$

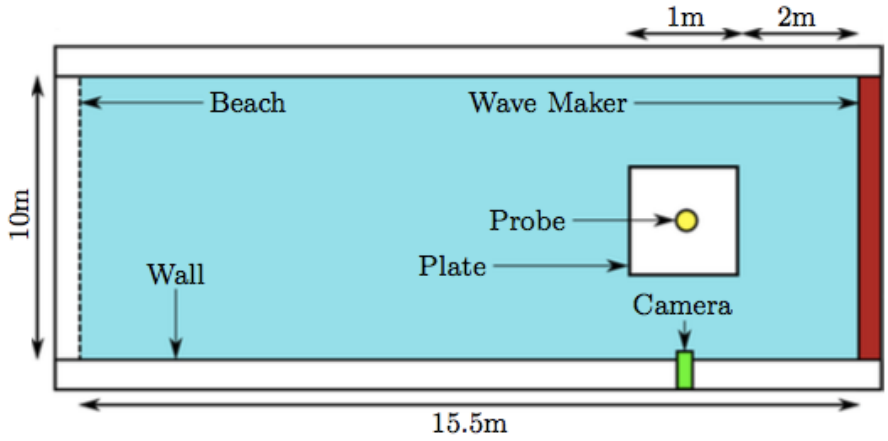

Figure 1: Plan view of experimental set-up (not to scale)

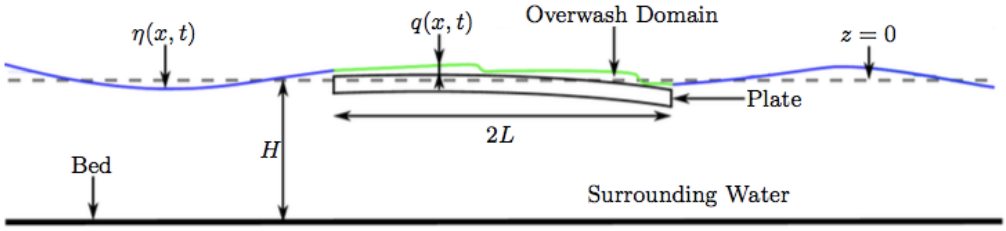

Figure 2: Schematic of overwash model (not to scale)

and elastic modulus $E = 750\,\mathrm{MPa}$. Following Montiel *et al.* (2013*a*,*b*) and Meylan *et al.* (2015) a reduced value of $E = 500\,\mathrm{MPa}$ is used to model the PVC plates. Three thicknesses were tested for each plastic: $h = 5\,\mathrm{mm}$, $10\,\mathrm{mm}$, $19\,\mathrm{mm}$ (PVC only) and $20\,\mathrm{mm}$ (PP only).

Regular incident waves with periods $T = 0.6\,\mathrm{s}$, $0.8\,\mathrm{s}$, and $1.0\,\mathrm{s}$ were used. The corresponding wavelengths are $\lambda = 0.56\,\mathrm{m}$, $1.00\,\mathrm{m}$ and $1.51\,\mathrm{m}$, respectively. Incident wave amplitudes A were chosen to provide steepnesses $kA = 0.04$, 0.08, 0.1, and 0.15. The wave number $k = 2\pi/\lambda$ is the positive real root of the dispersion relation $k\tanh(kH) = \omega^2/g$, where $\omega = 2\pi/T$ is angular frequency and $g \approx 9.81\,\mathrm{m\,s^{-2}}$ is gravitational acceleration.

A small wave probe and a high-definition video camera recorded the overwash. The camera provided a qualitative assessment of the overwash. The probe was positioned at the geometric centre of each plate's upper surface. It recorded time series of overwash depth at $120\,\mathrm{Hz}$ frequency, for $300\,\mathrm{s}$ following activation of the wave maker, which ran for over $300\,\mathrm{s}$. The series were analysed for the second $150\,\mathrm{s}$, as a conservative measure to cut off initial transients.

The probe detected overwash in 58 of the 72 tests conducted. The mean overwash depth was $1.77\,\mathrm{mm}$ over the 58 tests where overwash occurred. The maximum depth recorded was $9.95\,\mathrm{mm}$. Bores were a prominent feature in the overwash. The largest bores were generated at the plates' leading edges. The bores became turbulent and sometimes broke in deep overwash. The electronic supplementary material (ESM) shows two movies of overwash during tests in which the mean depth was $0.81\,\mathrm{mm}$ and $2.75\,\mathrm{mm}$, respectively.

3 Theoretical model

Let the Cartesian coordinate system (x, y, z) define locations in the basin. The coordinate (x, y) defines horizontal locations and its origin is the equilibrium plate centre. The incident waves travel in the positive x-direction. The coordinate z defines vertical locations and its origin is at the equilibrium water surface in the absence of plate cover.

The model is two-dimensional: (i) for simplicity; and (ii) as Meylan *et al.* (2015) found the motions of the plates are approximately uniform in the transverse dimension. It considers the geometry in the plane $y = 0$, and assumes motions in this plane are independent of the y-coordinate. Further, waves reflected by the basin boundaries are assumed to be negligible and, hence, the x-coordinate extends to infinity in its positive and negative directions.

Nonlinear shallow water theory models the overwash. Linear potential flow theory models the surrounding water. Kirchoff-Love thin plate theory models the plate. The plate and surrounding water motions are coupled. The wave elevation above the leading and trailing ends of the plate and its velocity there forces the overwash. The overwash does not affect the surrounding water or the plate motions (as motivated by Meylan *et al.*, 2015). Figure 2 shows a schematic of the model.

3.1 Coupled potential flow and floating thin plate model

Following potential flow theory, the water velocity field is defined as the gradient of a scalar potential function, i.e. $\mathbf{u} \equiv (u, w) = \nabla\Phi$. The water motion is assumed to be time-harmonic at the frequency of the incident wave, and thus $\Phi(x, y, t) = \mathrm{Re}\left\{\phi(x, z)\mathrm{e}^{-\mathrm{i}\omega t}\right\}$, where the (reduced) velocity potential ϕ is a complex-valued function.

Thin-plate theory allows the vertical motion of the plate to be defined in terms of the displacement of its lower surface, $z = \eta_\mathrm{p}(x, t)$. The motion is also assumed to be time-harmonic, and the displacement function is thus expressed as $\eta_\mathrm{p}(x, t) = \mathrm{Re}\left\{w(x)\mathrm{e}^{-\mathrm{i}\omega t}\right\}$. The model does not include lateral motions of the plate. The (reduced) displacement function, w, is decomposed into the orthonormal natural modes of vertical vibration of an in vacuo plate, $w_n(x)$ for $n = 0, 1, \ldots$, with, as yet unknown weights, ξ_n. Thus

$$w(x) = \sum_{n=0}^{\infty} \xi_n w_n(x), \qquad \text{where} \qquad w_0 = \frac{1}{\sqrt{2L}} \qquad \text{and} \qquad w_1 = \sqrt{\frac{3}{2L^3}}x \tag{1}$$

are the rigid-body modes, corresponding to heave and pitch, respectively, and

$$\begin{aligned} w_{2n} &= \frac{1}{\sqrt{2L}}\left(\frac{\cos\left(\mu_{2n}x\right)}{\cos\left(\mu_{2n}L\right)} + \frac{\cosh\left(\mu_{2n}x\right)}{\cosh\left(\mu_{2n}L\right)}\right) \qquad \text{and} \\ w_{2n+1} &= \frac{1}{\sqrt{2L}}\left(\frac{\sin\left(\mu_{2n+1}x\right)}{\sin\left(\mu_{2n+1}L\right)} + \frac{\sinh\left(\mu_{2n+1}x\right)}{\sinh\left(\mu_{2n+1}L\right)}\right) \end{aligned} \tag{2a}$$

for $n = 1, 2, \ldots$ are the even and odd flexural modes, respectively, with real eigenvalues $0 < \mu_n < \mu_{n+1}$ defined by

$$\tan\left(\mu_{2n}L\right) + \tanh\left(\mu_{2n}L\right) = 0 \quad \text{and} \quad \tan\left(\mu_{2n+1}L\right) - \tanh\left(\mu_{2n+1}L\right) = 0 \tag{3}$$

for $n = 2, 3, \ldots$, and $\mu_0 = \mu_1 = 0$ are defined for convenience.

Linear theory is employed. Thus, the problem is posed on the equilibrium domain. The velocity potential satisfies Laplace's equation in the equilibrium water domain, i.e.

$$\nabla^2\phi = 0 \quad \text{for} \quad -H < z < 0, \quad \text{where} \quad \nabla = (\partial_x, \partial_z). \tag{4a}$$

It also satisfies the impermeable bed and linearised free-surface conditions, respectively,

$$\partial_z\phi = 0 \quad \text{on} \quad z = -H \quad \text{and} \quad \partial_z\phi = \frac{\omega^2}{g}\phi \quad \text{on} \quad z = 0 \ \text{ for } \ x \notin (-L, L). \tag{4b}$$

In the far-field the velocity potential satisfies the radiation conditions

$$\phi \sim \frac{g}{\mathrm{i}\omega}\left(A\mathrm{e}^{\mathrm{i}kx} + R\mathrm{e}^{-\mathrm{i}kx}\right)\frac{\cosh k(z+h)}{\cosh(kh)} \quad \text{as} \quad x \to -\infty, \tag{4c}$$

$$\text{and} \qquad \phi \sim \frac{gT\mathrm{e}^{\mathrm{i}kx}\cosh k(z+h)}{\mathrm{i}\omega\cosh(kh)} \quad \text{as} \quad x \to \infty, \tag{4d}$$

where R and T are, as yet unknown, complex-valued reflection and transmission amplitudes, respectively.

The velocity potential and displacement function are coupled at their equilibrium interface via kinematic and dynamic conditions. The kinematic condition equates the vertical velocity of the water particles at the water surface to the vertical velocity of the corresponding points of the plate. The dynamic condition uses Kirchoff-Love thin-plate theory, and considers the vertical motions of the plate to be forced by the pressure differential between its upper and lower surfaces. The conditions assume the lower surface of the plate remains in contact with the water at all points and at all times during its motion. They are, respectively,

$$\partial_z\phi = -\mathrm{i}\omega\sum_{n=0}^{\infty}\xi_n w_n \qquad \text{and} \qquad \mathrm{i}\omega\phi = \sum_{n=0}^{\infty}\left\{1+\beta\mu_n^4-\omega^2\gamma\right\}\xi_n w_n \tag{4e}$$

on $z=0$ for $x\in(-L,L)$. Here, $\beta = Eh^3/\{12(1-\nu^2)\rho g\}$ and $\gamma = \rho_{\mathrm{p}}h/\rho g$ are scaled flexural rigidity and mass of the plate, respectively, where $\nu = 0.4$ and $\nu = 0.3$ are representative values of Poisson's ratio for PP and PVC, respectively. Coupling conditions (4e) use the frequently used zero-draught approximation (e.g. Meylan & Squire, 1994). Note that the Archimedean draught is used in § 3.3 to couple the surrounding water to the overwash.

The potential is expressed as the sum of scattering and radiation components, i.e.

$$\phi = \phi^{\mathrm{S}} - \mathrm{i}\omega\sum_{n=0}^{\infty}\xi_n\phi_n^{\mathrm{R}}. \tag{5}$$

The scattering potential ϕ^{S} satisfies the problem in which the plate is held in place, i.e. equations ($4a$–b) and the first component of equation (4e) with $\xi_n = 0$ set for all n. The radiation potential ϕ_j^{R} satisfies the problem in which the plate is forced to oscillate with unit amplitude in mode j in the absence of incident forcing, i.e. equations ($4a$–b) and the first component of equation (4e) with $\xi_n = \delta_{nj}$ and $A = 0$ set.

The component potentials are calculated using the free surface Green's function, $G(x-x_0,z)$. It is the solution of the governing equations, forced at the point $x = x_0$ on the free surface in the absence of plate cover and incident wave forcing, i.e.

$$\nabla^2 G = 0 \quad \text{for} \quad -H < z < 0, \quad \partial_z G = 0 \quad \text{on} \quad z = -H, \tag{6a}$$

$$\partial_z G - \omega^2 G/g = \delta(x-x_0) \quad \text{on} \quad z = 0, \tag{6b}$$

and the radiation condition that G represents outgoing waves in the far-field. Meylan & Squire (1994), for example, provide an explicit expression for a more general version of the Green's function. Green's theorem generates the integral equations

$$\phi^{\mathrm{S}}(x,0) = \frac{gA\mathrm{e}^{\mathrm{i}kx}}{\mathrm{i}\omega} - \frac{\omega^2}{g}\int_{-L}^{L} G(x-x_0,0)\phi^{\mathrm{S}}(x_0,0)\,\mathrm{d}x_0, \quad \text{and} \tag{7a}$$

$$\phi_n^{\mathrm{R}}(x,0) = -\int_{-L}^{L} G(x-x_0,0)\left(\frac{\omega^2}{g}\phi_n^{\mathrm{R}}(x_0) - w_n(x_0)\right)\mathrm{d}x_0 \quad \text{for} \quad n = 0,1,\ldots \tag{7b}$$

for $x \in (-L, L)$. The potentials are calculated numerically on the wetted surface of the plate, as the solutions of (7*a*–*b*). The radiation potentials, ϕ_n^{R}, are calculated for $n = 0, \ldots, N$, where N is finite and sufficiently large that the truncated version of (5) accurately approximates the full-linear solution.

Applying the second component of (4e) to the truncated potential and taking inner-products with respect to w_j for $j = 0, \ldots, N$, results in the system

$$\left(\mathbf{K} + \mathbf{C} - \omega^2\mathbf{M} - \omega^2\mathbf{A}(\omega) - \mathrm{i}\omega\mathbf{B}(\omega)\right)\boldsymbol{\xi} = \mathbf{f}(\omega). \tag{8}$$

Here, $\mathbf{K}$, $\mathbf{C}$ and $\mathbf{M}$ are diagonal stiffness, hydrostatic-restoring and mass matrices, respectively, $\mathbf{A}$ and $\mathbf{B}$ are added mass and damping matrices, respectively, $\mathbf{f}$ is the forcing vector, and $\boldsymbol{\xi}$ is a vector containing the modal weights. Their entries are defined as

$$\mathbf{K}_{jj} = \beta\mu_{j-1}^4, \quad \mathbf{C}_{jj} = 1 \quad \text{and} \quad \mathbf{M}_{jj} = \gamma \quad \text{for} \quad j = 1, \ldots, N+1, \tag{9a}$$

$$\omega^2\mathbf{A}_{ij} + \mathrm{i}\omega\mathbf{B}_{ij} = \frac{\omega^2}{g}\int_{-L}^{L} \phi_{j-1}^{\mathrm{R}}(x,0) w_{i-1}(x)\,\mathrm{d}x \quad \text{for} \quad i,j = 1, \ldots, N+1, \tag{9b}$$

$$\mathbf{f}_j = \frac{\mathrm{i}\omega}{g}\int_{-L}^{L} \phi^{\mathrm{S}}(x,0) w_{j-1}(x)\,\mathrm{d}x \quad \text{and} \quad \boldsymbol{\xi}_j = \xi_{j-1} \quad \text{for} \quad j = 1, \ldots, N+1. \tag{9c}$$

System (5) is solved for the vector of modal weights, $\boldsymbol{\xi}$. The reflection and transmission amplitudes are subsequently calculated as $R = AI_+$ and $T = A(1 + I_-)$, where

$$I_\pm = \frac{-\mathrm{i}\cosh^2(kH)}{\cosh(kH)\sinh(kH) + kH}\int_{-L}^{L} \mathrm{e}^{\pm\mathrm{i}kx}\left(\frac{\omega^2}{g}\phi(x,0) - \partial_z\phi(x,0)\right)\mathrm{d}x. \tag{10}$$

3.2 Nonlinear shallow water equations

It is assumed that (i) the vertical length scale of the overwash is much smaller than its horizontal length scale, (ii) the water particles' vertical accelerations are much smaller than gravitational acceleration and, thus, the water pressure is approximately hydrostatic, and (iii) the plate pitches at a small angle only. The assumptions are consistent with experimental observations. Assumption (ii) implies that the force of the plate's motion on the overwash is negligible in comparison to gravitational force. Assumption (iii) implies that the gravitational force acts approximately perpendicularly to the plate's upper surface. Further, turbulence and wave breaking are neglected as a simplifying assumption. Therefore, the nonlinear shallow water equations model the overwash, i.e. the hyperbolic partial differential system

$$\partial_t\mathbf{q} + \partial_x f(\mathbf{q}) = 0 \quad \text{for} \quad x \in (-L, L), \tag{11}$$

$$\text{where} \quad \mathbf{q} = [q, qu]^T \quad \text{and} \quad f(\mathbf{q}) = \left[qu, qu^2 + \frac{1}{2}gq^2\right]^T.$$

Here $u(x,t)$ is its depth averaged horizontal velocity and $q(x,t)$ is the overwash depth, which is defined as the height of the surface elevation above the plate's upper surface.

The numerical scheme outlined by Kurganov & Tadmor (2000) is used to approximate spatial derivatives in system (11). It is a second-order accurate finite volume method. It is able to capture bores which generate as discontinuities in the solution. In this numerical scheme, horizontal space is discretised into $M+1$ uniformly spaced cells centred at the points $\{x_0 = -L, x_1 = -L + \Delta x, \ldots, x_M = L\}$, and the notation $\mathbf{q}_j(t) \equiv \mathbf{q}(x_j, t)$ is employed. The spatial derivative in (11) is approximated as

$$\partial_x f(\mathbf{q}_j(t)) \approx -\mathcal{L}(\mathbf{q}_j(t)) = \frac{\mathbf{B}_{j+\frac{1}{2}}(t) - \mathbf{B}_{j-\frac{1}{2}}(t)}{\Delta x}, \tag{12}$$

where $\mathbf{B}_{j\pm\frac{1}{2}}$ are fluxes on the jth cell's left (-) and right (+) boundaries, defined via

$$\mathbf{B}_{j+\frac{1}{2}}(t) = \frac{a^+_{j+\frac{1}{2}} f(\mathbf{q}^-_{j+\frac{1}{2}}) - a^-_{j+\frac{1}{2}} f(\mathbf{q}^+_{j+\frac{1}{2}}) + a^+_{j+\frac{1}{2}} a^-_{j+\frac{1}{2}} \left(\mathbf{q}^+_{j+\frac{1}{2}} - \mathbf{q}^+_{j+\frac{1}{2}} \right)}{a^+_{j+\frac{1}{2}} - a^-_{j+\frac{1}{2}}}, \tag{13}$$

$$\text{where} \quad a^\pm_{j+\frac{1}{2}} = \pm \max \left\{ \pm\kappa_\pm(\mathbf{q}^-_{j+\frac{1}{2}}), \pm\kappa_\pm(\mathbf{q}^+_{j+\frac{1}{2}}), 0 \right\} \quad \text{and} \quad \kappa_\pm(\mathbf{q}) = u \pm \sqrt{gq}, \tag{14}$$

i.e. $\kappa_\pm(\mathbf{q})$ are the largest (+) and smallest (-) eigenvalues of the Jacobian of $f(\mathbf{q})$.

The minmod limiter presented in Kurganov & Tadmor (2000) is used to prevent unnatural oscillations occurring either side of a shock, where

$$\text{minmod}\left\{\bullet_1, \bullet_2, \dots\right\} = \begin{cases} \min_j\{\bullet_j\} & \text{if } \bullet_j > 0 \quad \text{for all } j, \\ \max_j\{\bullet_j\} & \text{if } \bullet_j < 0 \quad \text{for all } j, \end{cases} \tag{15}$$

and zero otherwise. It determines

$$\mathbf{q}_{x,j+\frac{1}{2}} = \text{minmod}\left\{ \theta \frac{\mathbf{q}_{j+1} - \mathbf{q}_j}{\Delta x}, \frac{\mathbf{q}_{j+1} - \mathbf{q}_{j-1}}{2\Delta x}, \theta \frac{\mathbf{q}_j - \mathbf{q}_{j-1}}{\Delta x} \right\}, \tag{16}$$

where $\theta = 1.5$, which, in turn, determines the half-space values

$$\mathbf{q}^+_{j+\frac{1}{2}} = \mathbf{q}_{j+1} - \frac{1}{2}\mathbf{q}_{x,j+\frac{1}{2}} \qquad \text{and} \qquad \mathbf{q}^-_{j+\frac{1}{2}} = \mathbf{q}_j + \frac{1}{2}\mathbf{q}_{x,j+\frac{1}{2}} \tag{17}$$

used in equations (13) and (14).

The total variation diminishing Runge-Kutta 2 scheme is used to time step. It suppresses unnatural extrema as the solution evolves. The scheme is expressed as

$$2\mathbf{q}_j\,(t + \Delta t) = 2\mathbf{q}_j(t) + \Delta t \mathcal{L}(\mathbf{q}_j(t)) + \Delta t \mathcal{L}\big(\mathbf{q}_j(t) + \Delta t \mathcal{L}(\mathbf{q}_j(t))\big) \tag{18}$$

where $\Delta t > 0$ is a time step satisfying the CFL condition (Gottlieb & Shu, 1998).

3.3 Forcing the shallow water equations

The coupled potential-flow/thin-plate model provides steady forcing for the shallow water equations. It defines two conditions at each end of the interval occupied by the shallow water. This is a sufficient number of boundary conditions for the shallow-water equations. It allows for bores to be generated at the ends of the plate and also permits water to enter and exit the interval.

The overwash depth at the interface with the surrounding water is equated to the height of the free surface elevation, $\eta(x,t) = \rho\partial_t\Phi(x,0,t)/g$, above the upper surface of the plate. It is set to zero if the height is negative. Thus,

$$q(\pm L, t) = \max\left\{\eta(\pm L, t) - \eta_\text{p}(\pm L, t) + C, 0\right\}, \quad \text{where} \quad C = h(1 - \rho_\text{p} \,/\, \rho) \tag{19}$$

is the plate's equilibrium freeboard, which is calculated via Archimedes' principle. Numerical tests showed evanescent wave motions have minor impact on the results presented in § 4. Thus, the free surface elevations are approximated as

$$\eta(-L,t) \approx \text{Re}\left\{\left(A\mathrm{e}^{-ikL} + R\mathrm{e}^{ikL}\right)\mathrm{e}^{-i\omega t}\right\} \quad \text{and} \quad \eta(L,t) \approx \text{Re}\left\{T\mathrm{e}^{ikL - i\omega t}\right\}. \tag{20}$$

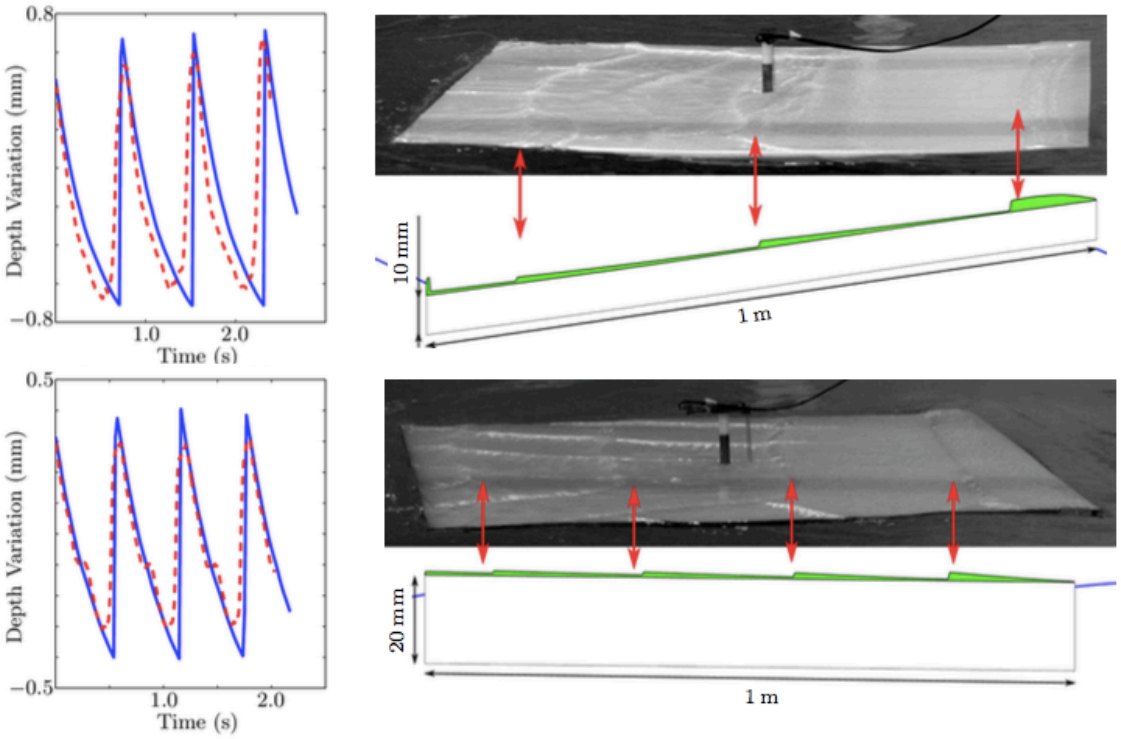

Figure 3: Left-hand panels show variation from mean of overwash depth signal measured during experiments (dashed red curves) and predicted by theoretical model (solid blue) from an arbitrary initial time. Right-hand panels compare snapshots of model simulations with photos of corresponding experiments. Red arrows highlight locations of corresponding bores. Note that, in the simulation snapshots, the vertical and horizontal lengths are on different scales. Top panels are results for 10 mm thick PVC plate forced by waves of steepness $kA = 0.10$ and length $\lambda = 1.00\,\mathrm{m}$. Bottom panels are results for 20 mm thick PP plate forced by waves of steepness $kA = 0.08$ and length $\lambda = 0.56\,\mathrm{m}$.

Similarly, the horizontal velocity of the overwash at the interface with the surrounding water is equated to the horizontal velocity of the free surface water particles adjacent to the plate edges, $U(x,t) = \partial_x \Phi(x,0,t)$. It is set to zero if the free surface is not above the plate's ends. Thus

$$u(\pm L, t) = \begin{cases} U(\pm L, t) & \text{if } \eta(\pm L, t) \geq -\eta_{\mathrm{p}}(\pm L, t) + C, \\ 0 & \text{otherwise.} \end{cases} \tag{21}$$

Initially, the shallow water is set to a uniform depth of $q = 1\,\mu\,\mathrm{m}$ and to be stationary, i.e. $u = 0$. For a prescribed incident wave and plate, the shallow water equations are run to a quasi-steady state, i.e. until the overwash depth profile is approximately time-harmonic. For the results shown in § 4, this occurred after approximately 40 wave periods.

4 Results

The model accurately predicts the presence of overwash at the centre of the plate for the 58 test conditions the gauge detected it in the experiments. It predicts overwash for four of the 14 test conditions in which overwash was not detected in the experiments.

Figure 3 shows example qualitative comparisons of overwash predicted by the model and recorded during the experiments. The example tests are for a 10 mm thick PVC plate forced by waves of

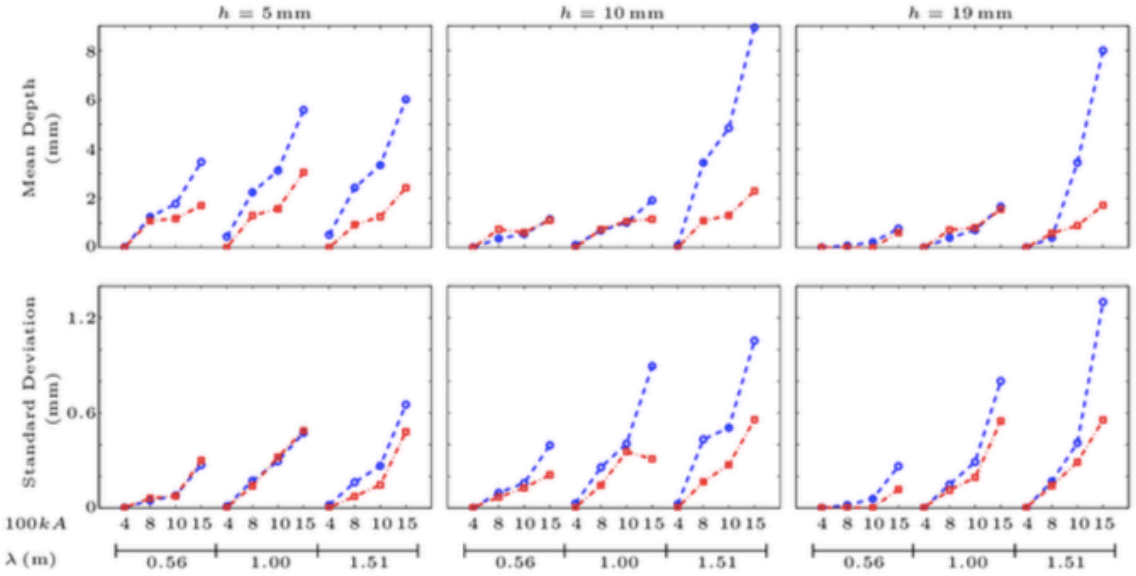

Figure 4: Overwash mean depth and standard deviation at the centre of each PVC plate's upper surface. Blue circles denote theoretical model predictions. Red squares denote values extracted from experimental data.

steepness $kA = 0.10$ and length $\lambda = 1.00\,\mathrm{m}$ (top panels), and a 20 mm thick PP plate forced by waves of steepness $kA = 0.08$ and length $\lambda = 0.56\,\mathrm{m}$ (bottom).

The left-hand panels show the variation of overwash depth about its mean depth at the plate's centre. Bores are evident in the signals. The model predicts the shape and amplitude of the bores accurately, although it is unable to capture the rounded peaks in the experimental signal. Small bores generated at the sides of the PVC plate cause the shoulders in its experimental signal.

The right-hand panels show snapshots of the overwash profile predicted by the model and photos from the corresponding tests. Note that the direction of the incident wave has been reversed in the model to match the experiments, and that, in the simulation snapshots, the horizontal and vertical lengths are on different scales. Red arrows indicate the location of corresponding bores in the model and experiments. They show that the model predicts the distance between successive bores accurately. The ESM provides movie comparisons for the two tests. They emphasise that the model predicts the bore velocities accurately.

Overwash is quantified in terms of the mean and standard deviation of the depth signal at the centre of the plate. Figure 4 compares the model predictions of these quantities with the values extracted from the experimental measurements. The data are separated into different incident wavelengths and presented as functions of incident steepness. Results are shown for the PVC plate tests only, as the behaviours are indicative of those for the PP plate tests, which are contained in the ESM.

The mean depth and standard deviation increase as the incident steepness increases. Further, for the two thicker plates, $h = 10\,\mathrm{mm}$ and 19 mm, the depth and deviation tend to increase as incident wavelength increases. Model predictions (not shown) indicate that overwash dies out as the incident wavelength increases beyond the values tested here.

The model predicts the depth and deviation accurately for the smallest incident wavelength, $\lambda = 0.56\,\mathrm{m}$, except for the test using the thinnest plate and steepest incident wave, $h = 5\,\mathrm{mm}$ and $kA = 0.15$. Neglecting this isolated case, the mean error is 0.16 mm for the depth and 0.04 mm for the deviation. Further, the model is accurate for the intermediate wavelength, $\lambda = 1.00\,\mathrm{m}$, and the two thicker plates, with the exception of the steepest incident wave for the 10 mm thick plate. For the

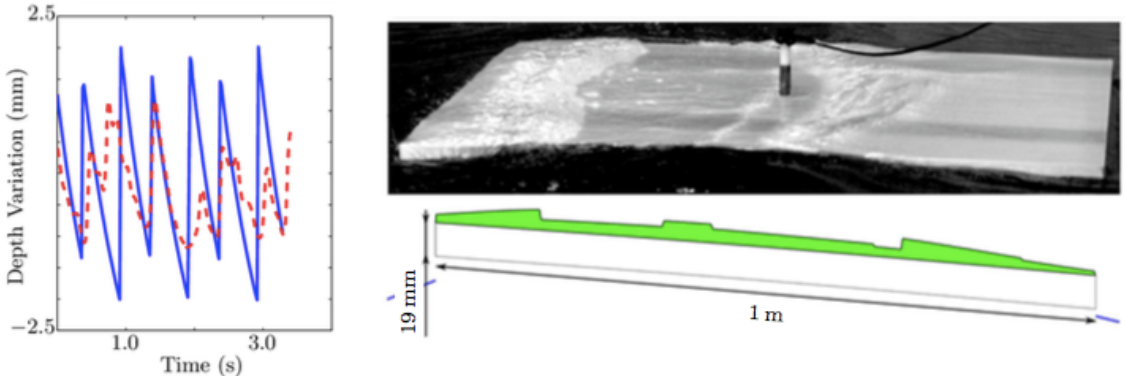

Figure 5: As in figure 3 for a 19 mm thick PVC plate forced by waves of steepness $kA = 0.15$ and length $\lambda = 1.56$ m.

thinnest plate, the model is accurate only for the least steep incident wave.

The model increasingly over predicts the depth and deviation as the incident wave becomes steeper and longer, i.e. the overwash becomes deeper and more variable. The over prediction is significant in some of the tests using the longest incident wavelength, $\lambda = 1.56$ m. For example, for the longest wavelength, the mean error is 2.44 mm for the depth and 0.19 mm for the deviation.

Figure 5 shows a qualitative model-experiment comparison, which is typical of the regime where the model over predicts the depth and deviation. The ESM contains the corresponding movies. The photo shows large and turbulent bores in the experiments, which are generated at the trailing end of the plate as well as at the leading end. The photo shows an instant when the bores collided, which caused them to break. The model snapshot shows it predicts bores are generated at both plate ends. However, it shows the shallow water equations permit the bores to pass through one another (the mound approximately one-third of the plate length in from the left-hand end). Turbulence and breaking lead to the significant differences in the depth variations shown in the left-hand panel. Note the variation conceals the 6.64 mm difference in the mean depths for this test.

5 Conclusions

A theoretical model of overwash of a thin floating plate, forced by regular incident waves, has been presented. It extends the linear potential-flow/thin-plate model of coupled wave and plate motions, which neglects overwash, using the nonlinear shallow water equations to model the overwash. It was validated via laboratory experimental measurements of the overwash depth on thin floating plastic plates.

The model was shown to predict qualitative and quantitative overwash properties accurately for shallow overwash, which generally occurs for incident waves with relatively short lengths or low steepnesses. This implies that, in this regime, the linear potential-flow/thin-plate model accurately predicts overwash forcing and the shallow water equations accurately model the overwash. Further, the model was shown to over predict the overwash depth and deviation increasingly, as the overwash becomes deeper, i.e. the incident wave becomes longer or steeper. This was shown to coincide with the experimental regime in which large turbulent bores are generated at both the plates' leading and trailing ends and break when they collide. This implies a turbulent version of the shallow water equations will improve model accuracy for long, steep incident waves.

The model, or an extended version of it, has the potential to act as the basis of a model of the impact of overwash on wave transmission, as observed in laboratory experiments by Bennetts & Williams (2015) and Bennetts *et al.* (2015). This model, in turn, has the potential to predict the

amplitude dependence of the attenuation rate of ocean waves in the ice-covered ocean with respect to distance travelled, which was shown by Meylan *et al.* (2015) using in-situ measurements of wave activity. However, as noted in § 1, the laboratory experiments only validate the model for plates that have rigidities representative of sea ice floes at field scale up to limited geometric length scales. Moreover, the turbulence observed in the overwash during the experiments implies that the Reynolds number is an important quantity to evaluate the overwash properties at field scale. As the Reynolds number scales with the characteristic length to the power three-halves, the onset of turbulence is expected for relatively shallower overwash.

Plymouth University funded the experiments. Peter Arber, Claudio Cavaliere and Alberto Alberello helped conduct the experiments. An Australian Postgraduate Award funds a PhD scholarship for DMS. The Australian Research Council funds an early-career researcher fellowship for LGB (DE130101571). The Australian Antarctic Science Program funds LGB and DMS (Project 4123). The U.S. Office of Naval Research supports MHM (Grant N00014-13-1-0290).

References

Bennetts, L. G., Alberello, A., Meylan, M. H. Cavaliere, C. Babanin, A. & Toffoli, A. 2015 An idealised experimental model of ocean surface wave transmission by an ice floe. *Ocean Model.* doi:10.1016/j.ocemod.2015.03.001.

Bennetts, L. G. & Williams, T. D. 2010 Wave scattering by ice floes and polynyas of arbitrary shape. *J. Fluid Mech.* **662**, 5–35.

Bennetts, L. G. & Williams, T. D. 2015 Water wave transmission by an array of floating disks. *Proc. R. Soc. Lond. A* **471** (2014069).

Buchner, B. & Cozijn, J. L. 1997 An investigation into the numerical simulation of green water. In *Proc. Int. Conference on the Behaviour of Offshore Structures*, vol. 2, pp. 113–125. Delft: Elsevier Science.

Doble, M. J. & Bidlot, J.-R. 2013 Wavebuoy measurements at the Antarctic sea ice edge compared with an enhanced ECMWF WAM: progress towards global waves-in-ice modeling. *Ocean Model.* **70**, 166–173.

Dumont, D., Kohout, A. L. & Bertino, L. 2011 A wave-based model for the marginal ice zone including a floe breaking parameterization. *J. Geophys. Res.* **116** (C04001).

Gottlieb, S. & Shu, C. W. 1998 Total variation diminishing Runge-Kutta schemes. *Math. Comp.* **67** (221), 73–85.

Greco, M. 2001 A two-dimensional study of green-water loading. PhD thesis, Norwegian University of Science and Technology.

Kurganov, A. & Tadmor, E. 2000 New high-resolution central schemes for nonlinear conservation laws and convection–diffusion equations. *J. Comput. Phys.* **160** (1), 241–282.

Meylan, M. H., Bennetts, L. G., Alberello, A., Cavaliere, C. & Toffoli, A. 2015 Experimental and theoretical models of wave-induced flexure of a sea ice floe. *Phys. Fluids* **27**, 041704.

Meylan, M. H., Bennetts, L. G. & Kohout, A. L. 2014 In-situ measurements and analysis of ocean waves in the Antarctic marginal ice zone. *Geophys. Res. Lett.* **41**(14), 5046–5051.

Meylan, M. H. & Squire, V. A. 1994 The response of ice floes to ocean waves. *J. Geophys. Res.* **99** (C1), 891–900.

Mizoguchi, S. 1989 Analysis of shipping water with the experiments and the numerical calculations. *J. Soc. Nat. Nav. Archit. Jpn.* **27**, 83–91.

Montiel, F., Bonnefoy, F., Ferrant, P., Bennetts, L. G., Squire, V. A. & Marsault, P. 2013*a* Hydroelastic response of floating elastic disks to regular waves. Part 1: Wave tank experiments. *J. Fluid Mech.* **723**, 604–628.

Montiel, F., Bennetts, L. G., Squire, V. A., Bonnefoy, F. & Ferrant, P. 2013*b* Hydroelastic response of floating elastic disks to regular waves. Part 2: Modal analysis. *J. Fluid Mech.* **723**, 629–652.

Papathanasiou, T. K., Karperaki, A., Theotokoglou, E. E. & Belibassakis, K. A. 2015 A higher order FEM for time-domain hydroelastic analysis of large floating bodies in an inhomogeneous shallow water environment. *Proc. R. Soc. Lond. A* **471** (2173).

Squire, V. A. 2007 Of ocean waves and sea-ice revisited. *Cold Reg. Sci. Technol.* **49**, 110–133.